Research in Astronomy and Astrophysics, 23:075009 (8pp), 2023 July https://doi.org/10.1088/1674-4527/accdc4

The Study of Helium Variations in Star Clusters Using China Space Station Telescope

Xin Ji[1,2], Licai Deng[1,2,3,*], Yang Chen[4,1], Chengyuan Li[3,5], and Chao Liu[1,2]
[1] Key Laboratory for Optical Astronomy, National Astronomical Observatories, Chinese Academy of Sciences, Beijing 100101, China; licai@nao.cas.cn, cy@ahu.edu.cn, jixin@nao.cas.cn, liuchao@nao.cas.cn
[2] School of Astronomy and Space Science, University of Chinese Academy of Sciences, Beijing 100101, China
[3] Department of Astronomy, School of Physics and Astronomy, China-West Normal University, Nanchong 637009, China; lichengy5@mail.sysu.edu.cn
[4] Anhui University, Hefei 230601, China
[5] School of Physics and Astronomy, Sun Yat-sen University, Zhuhai 519082, China
Received 2023 March 12; revised 2023 April 10; accepted 2023 April 13; published 2023 June 15

Abstract

The China Space Station Telescope (CSST) is a 2 m space-based optical-UV telescope. Its primary goal is to carry out a high-resolution photometric imaging survey of a 17,500 square degree sky area using the on board Survey Camera. With its wide field of view (1.1 square degrees) and a mosaic imager containing 640 million pixels, studying the different populations of stars within star clusters is highly feasible. The aim of this study is to assess the CSST's ability to distinguish between stellar populations with varying helium abundance levels, with the help of Modules for Experiments in Stellar Astrophysics. The results of the CSST's photometry for these different populations are presented by transferring the models into the CSST Survey Camera photometric system. The findings confirm that helium-enriched stellar populations will have unique patterns in the color–magnitude diagrams under the CSST photometric system, compared to normal stellar populations. The CSST, with its filters and wide field of view of the Survey Camera, provides a new avenue for the study of multiple populations in star clusters.

Key words: (Galaxy:) globular clusters: general – stars: abundances – (stars:) Hertzsprung-Russell and C-M diagrams

1. Introduction

A star cluster is a stellar system composed of a large number of gravitationally bound stars that are formed from a single progenitor giant molecular cloud at approximately the same time through a single burst. Star clusters are thus considered as the basic units of star formation (Lada & Lada 2003). This fact therefore suggests a "simple stellar population" (SSP) scenario. The scenario indicates that stars in a cluster should share the same age and chemical composition, especially the major elements hydrogen and helium. However, in recent decades multiple populations (MPs) have been detected in various types of star clusters, including most of the old globular clusters (GCs) (e.g., Carretta et al. 2009; Niederhofer et al. 2017; Milone et al. 2020) and some of the intermediate-age clusters in the Magellanic Clouds (MC) (e.g., Martocchia et al. 2018; Li & de Grijs 2019; Saracino et al. 2019), which have been intensively observed by Hubble Space Telescope (HST) and large ground-based facilities.

One of the main characteristics of MPs is the star-to-star chemical variations of light elements, including He, C, N, O, Na, Mg and Al. These elements are affected by several nuclear reactions during hydrogen-burning, such as the proton-capture process that leads to the well-known Na-O and Mg-Al anti-correlations (Shetrone 1996; Gratton et al. 2004; Carretta et al. 2009) and CNO cycle that causes the enhancement of N and depletion of C and O. Thanks to the high resolution HST ultraviolet (UV)-optical observations, these MPs can be observed through imaging using pseudo-color–magnitude diagrams (CMDs) and chromosome maps defined in Milone et al. (2015), and which were also used in Piotto et al. (2015) and Milone et al. (2017). The direct product of hydrogen-burning, helium, should be enhanced and can be modeled for clusters showing MP signatures (Bastian & Lardo 2018). However, the direct measurement of helium abundance is a challenge due to helium's ionization energy. For old GCs in the Galaxy, only a limited number of horizontal branch (HB) stars can have effective temperatures ($T_{\rm eff}$) around ~8000–11,500 K, that are high enough to show helium lines in near-ultraviolet (NUV) (e.g., Villanova et al. 2009; Marino et al. 2014). An alternative method is indirect exploration via deep photometry. He-enrichment will increase the mean molecular weight and decrease the opacity, and thus increase the nuclear reaction rates. As a result, the stars with higher helium abundance will evolve faster and be brighter and hotter than their helium-normal counterparts at each stage, which can be detected by photometric observations. Fast evolution of He-enriched stars will

* Corresponding author.

let them reach an advanced evolutionary stage earlier, making later branches of star clusters containing stars with different masses for different He abundances. However, He determination via stars with later evolution phases, such as HB stars (e.g., Dalessandro et al. 2011; Gratton et al. 2013; Chantereau et al. 2019), is often overestimated, as later generations of stars may undergo more mass loss than earlier generations (Tailo et al. 2020). Therefore the photometric measurement of helium should use stars which have experienced less mass loss, especially the dwarf stars on the main sequence (MS), which require deeper photometry (Li 2021).

The China Space Station Telescope (CSST) is a 2 m space telescope which is scheduled to be launched in 2024. There are two imaging instruments on board, namely the Survey Camera (SC) and the Multi-Channel Imager (MCI). The MCI is designed to have more filters with narrow bandwidth and is scheduled for deeper exposures than those for the SC. On the other hand, the SC has a much larger field of view (FOV, $\sim$1.1 deg^2) than the MCI ($7\farcm5 \times 7\farcm5$). With both imaging instruments, CSST will provide high spatial resolution ($\sim 0\farcs15$ and $0\farcs18$ at 633 nm for SC and MCI, respectively) images in multi-band filters covering a wide wavelength range from NUV to near-infrared (NIR). The SC will perform a photometric survey of a sky area of $\sim$17,500 deg^2 in a 10 yr mission (Zhan 2011; Cao et al. 2018; Gong et al. 2019). In this article, we focus on the role of the SC for detecting MPs of star clusters. For the MCI's function in this context, we recommend the comprehensive discussions in Li et al. (2022).

Given the advantages of the SC/CSST instrument in both wavelength coverage and FOV, it is expected that the CSST will have a great impact on the physics of star clusters. In this work, we are going to tackle the challenging issues of MPs resulting from variations of stellar chemical compositions in star clusters. We take the GC NGC 2808 as a prototype in this work, which is known for its triple MSs with dramatic helium differences (Piotto et al. 2007). We will build isochrones with different helium contents from MS to advanced evolutionary stages until HB, and then test the capability of CSST instruments in terms of helium abundance variations.

This article is organized as follows: In Section 2 we introduce the main parameters of the SC/CSST instrument and the details of our methods for building the cluster model and converting it to the CSST photometry system. The stellar models with different helium content and their observational properties are presented in Section 3. Discussions of the results and conclusions will be presented in Section 4.

2. Modeling Stellar Populations Under the CSST Photometric System

The grand science plan of CSST covers most of the cutting edge studies in all branches of astrophysics, including a high spatial resolution large sky survey using the SC, which is optimized toward NUV. The SC has seven broad-band photometric filters, namely *NUV, u, g, r, i, z, y* (filter parameters are listed in Table 1). Figure 1 demonstrates the photometry system of SC, overplotted with a typical MS dwarf star and its helium-enriched counterpart. It is clear to see from Figure 1 that the main features of helium enhancements are well sampled by filters in shorter wavelengths, including helium lines and enhanced continuum. The goal of this article is to study if the CSST can reveal stellar populations with different helium abundances, as mentioned above. The scientific merit in the context of MPs in star clusters is just like the MCI as thoroughly described in Li et al. (2022).

Table 1
Key Parameters of the SC/CSST Filters

Filter	Exposure Time/s	Wavelength Range/nm	Limiting Magnitude/mag
NUV	4 × 150 s	252 ∼ 321	25.4
u	2 × 150 s	321 ∼ 401	25.4
g	2 × 150 s	401 ∼ 547	26.3
r	2 × 150 s	547 ∼ 692	26.0
i	2 × 150 s	692 ∼ 842	25.9
z	2 × 150 s	842 ∼ 1080	25.2
y	4 × 150 s	927 ∼ 1080	24.4

As the primary survey instrument on board CSST, SC has fewer filters than MCI, but it has a significantly larger FOV. Figure 2 illustrates the FOV of SC, MCI and Wide Field and Planetary Camera 2 (WFPC2)/HST, by the blue, red and gray squares or a polygon respectively. As we will introduce below, in this work we take NGC 2808 as an example target, we therefore use the sky image with NGC 2808 in the center. The tidal radius of the cluster NGC 2808 $\sim 9\farcm1$ (Moreno et al. 2014) is also indicated by the circle. Given the ultra-deep photometry of SC/CSST, faint objects beyond the dynamical radius of star clusters can be captured with single exposures. Compared with MCI/CSST (Li et al. 2022) in the context of FOV and survey efficiency, SC will provide a unique capability to sample all star members from different structures of star clusters, such as those in the outskirts that are undergoing dynamical evaporation, or stars in tidal tails of clusters.

NGC 2808 has been confirmed to have significant helium abundance variations (Piotto et al. 2007). To mimic MPs for an NGC 2808-like cluster, we need to derive its basic parameters. High spatial resolution images were collected through WFPC2 on board the HST (GO-6804 program, PI: F, Fusi Pecci), which are available from the HST archive. We derived photometry results of NGC 2808 using the DOLPHOT[6] stellar photometry package with its WFPC2 module. We ran the wfpc2mask, splitgroups, calcsky and dolphot tasks in series, following the preprocessing steps recommended in the DOLPHOT/WFPC2

[6] DOLPHOT is a stellar photometry package adapted from HSTphot for general use. See http://americano.dolphinsim.com/dolphot for more information.

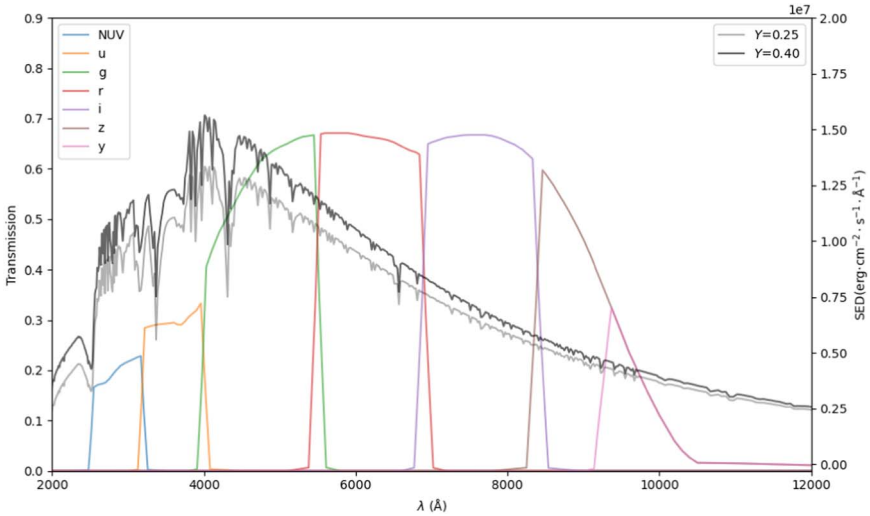

Figure 1. The transmission curves for SC/CSST filters with the vertical axis on the left, and the filter IDs in the insets. Two example spectra of typical dwarf MS stars ($T_{\rm eff} \sim 6300$ and lg$g \sim 4.4$) for helium normal (thin black line) and enriched dwarfs (thick black line) are plotted with the flux scale on the right.

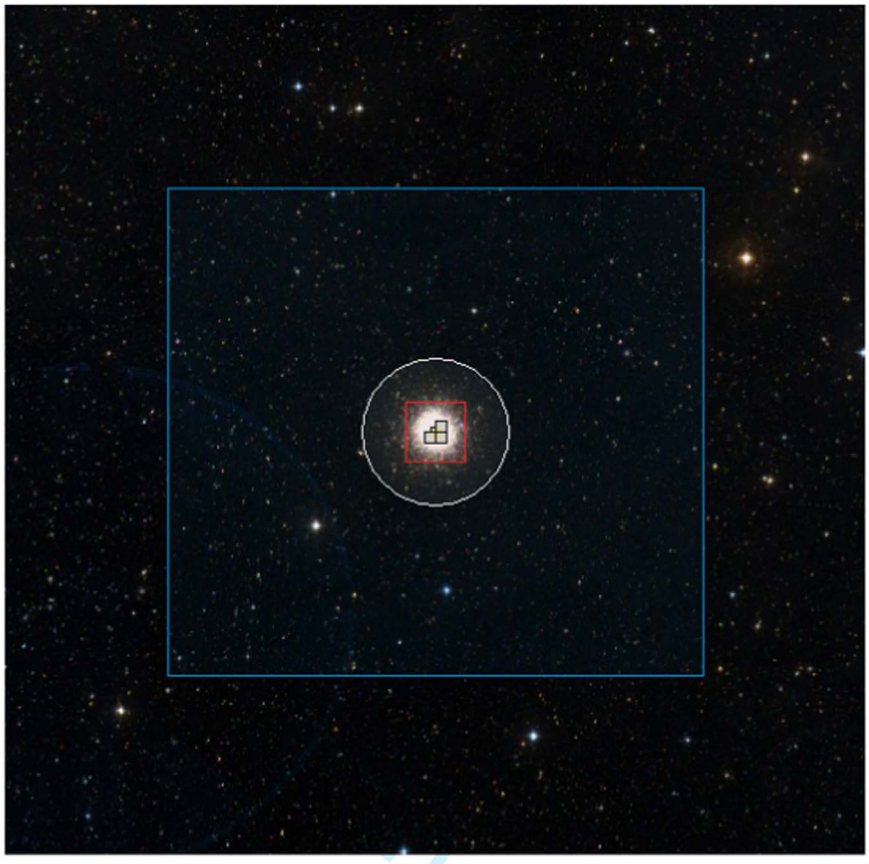

Figure 2. Comparison of FOV of CSST instrument and NGC 2808's tidal radius. The blue square signifies the FOV of SC/CSST on the sky, red square displays that of MCI/CSST and white circle indicates the tidal radius of NGC 2808. FOV of HST/WFPC2 is also plotted as reference in the center with a black border.

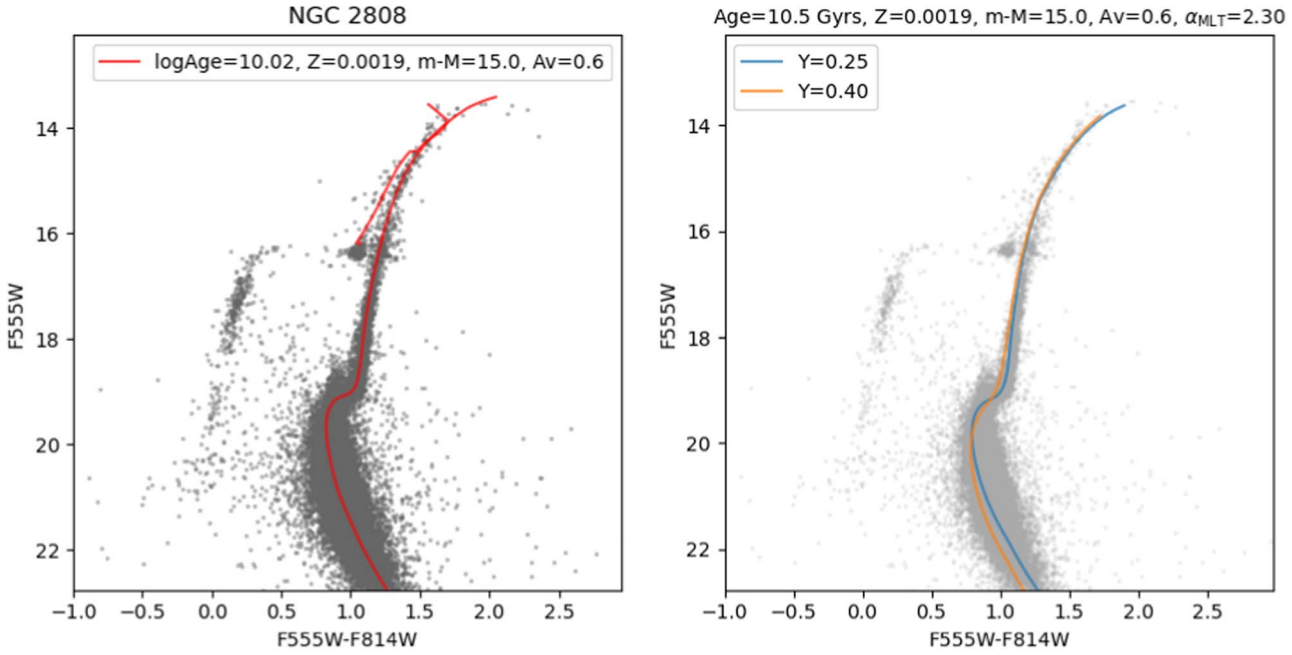

Figure 3. Left panel: isochrone fitting of NGC 2808, with parameters shown in the label, which are similar to those in Massari et al. (2016). Right panel: The two isochrones converted into HST/WFPC2 filters by PARSEC bolometric corrections, the blue curve is for $Y = 0.25$ and the orange one for $Y = 0.40$, overplotted on the observations of NGC 2808.

Users Guide (Dolphin 2016) to yield the best photometric results. The output files of DOLPHOT include several parameters to estimate the quality of our photometry, including signal-to-noise ratio (SNR), Object sharpness, Object roundness, Crowding, Object type and Magnitude uncertainty. For this research, we select stars with $|\text{Object sharpness}| < 0.1$, Crowding < 0.5 mag and Magnitude uncertainty < 0.2 mag to ensure that our photometric data have high enough quality (Monelli et al. 2010).

After generating photometry results of NGC 2808, we derived the basic cluster parameters by fitting the PARSEC isochrones (Bressan et al. 2012) to the observational data. The results are demonstrated in the left panel of Figure 3. The best fit parameters are: lgAge $= 10.02$, $Z = 0.0019$, distance modulus $(m - M)_0 = 15.0$ mag and extinction $A_V = 0.60$ mag. They are all in good agreement with previous studies (Massari et al. 2016).

In order to understand the properties of star clusters that are linked to possible helium variations, and to check the feasibility of CSST photometry for such a study, we built models with the observed properties of the cluster with the Modules for Experiments in Stellar Astrophysics (MESA), choosing two sets of helium abundances $Y = 0.25$ and $Y = 0.40$ as inferred by previous studies (Piotto et al. 2007). The initial mass of the isochrones varies from 0.500 to 0.873 $M_\odot$ and 0.400–0.657 $M_\odot$ for each Y of the helium abundance. Other input physics were mainly taken from Choi et al. (2016), which describes the MESA Isochrones and Stellar Tracks (MIST) project as applicable here.[7] As shown in Table 2, some minor adjustments were made to fit our specific science goals. We ran each model with their initial mass, initial helium content Y and initial metallicity Z (0.0019 from the isochrone fitting) from protostar to the cluster age (roughly 10.5 Gyr from the isochrone fitting). While running directly with the MIST parameters, we found that some branches of the resulting isochrones, especially the red giant branch (RGB), are significantly redder than observations, which indicate that some parameters from Choi et al. (2016) (especially the convection parameter $\alpha_{\rm MLT}$) do not really fit NGC 2808. So, we modify the $\alpha_{\rm MLT}$ to get better fitting of the isochrones. Finally, we choose $\alpha_{\rm MLT} = 2.30$, as shown in Table 2, which best reproduces the observed RGB colors. The right panel of Figure 3 features a comparison of our model isochrones, converted into HST/WFPC2 filters by PARSEC bolometric corrections,[8] with the observation of NGC 2808. The final results of the isochrones built using the grid of stellar tracks are depicted in the right panel of Figure 3.

The two isochrones with the two initial helium abundances Y were then transformed from the theoretical frame into the CSST photometric system. We computed the stellar atmosphere models and spectra for these models with ATLAS12 code and SYNTHE (Kurucz 2005). Based on this spectral library, we

[7] http://waps.cfa.harvard.edu/MIST/
[8] http://stev.oapd.inaf.it/YBC

Table 2
The Parameters of Input Physics For Modeling, Mainly from Choi et al. (2016), which Describes the MIST Project

Ingredient	Adopted Prescriptions and Parameters
Equation of state	OPAL+SCVH+MacDonald+HELM+PC
Opacity	OPAL Type I for $\log T \gtrsim 4$; Ferguson for $\log T \lesssim 4$; Type I $\rightarrow$Type II at the end of H burning
Reaction Rates	JINA REACLIB
Boundary Conditions	ATLAS12; $\tau = 100$ tables + photosphere tables + gray atmosphere
Diffusion	Track five "classes" of species; MS only
Radiation Turbulence	$D_{\rm RT} = 1$
Rotation	solid-body rotation at ZAMS with $v_{\rm ZAMS}/v_{\rm crit} = \Omega_{\rm ZAMS}/\Omega_{\rm crit} = 0.4$
Convection: Ledoux + MLT	$\alpha_{\rm MLT} = 2.30$, $\nu = 1/3$, $y = 8$
Overshoot	time-dependent, diffusive, $f_{\rm ov,\ core} = 0.0160$, $f_{\rm ov,\ env} = f_{\rm ov,\ sh} = 0.0174$
Semiconvection	$\alpha_{\rm sc} = 0.1$
Thermohaline	$\alpha_{\rm th} = 666$
Mass Loss: Low Mass Stars	$\dot{M}_{\rm R} = 4 \times 10^{-13} \eta_{\rm R} \frac{(L/L_\odot)(R/R_\odot)}{M/M_\odot}\ M_\odot\ {\rm yr}^{-1}$; $\eta_{\rm R} = 0.1$ for the RGB
Mass Loss: Rotational	$\xi = 0.43$, boost factor capped at 10^4, $\dot{M}_{\rm max} = 10^{-3}\ M_\odot\ {\rm yr}^{-1}$

Note. $\alpha_{\rm MLT}$ is taken from our modeling.

convert the `log_L` and `log_Teff` into the observational frame of CSST photometry system by following the process described in Chen & Girardi (2019).

For stars that evolved off the RGB-tip, the dredge-up and mass loss make the surface abundance pattern more complicated. We tried using MESA to build a series of models with all parameters describing such factors with a fixed metallicity, changing only helium content (and hydrogen content accordingly, to mimic gas recycling due to massive star evolution at the early stages of the population). The results show that stars after helium flash, including those at the core helium burning stage on the HB, do not really behave monotonically with the helium abundance. As a matter of fact, the evolutionary stages of stars beyond the RGB-tip depend critically on several other factors, such as rotation, mass loss rates (which can also resemble the mass exchange in contact binary systems) and the treatment of overshoot parameters during the previous stages, which give rise to more uncertainties and make the initial He abundance a less important factor. Therefore we limited our discussions from MS phase until the tip of RGB.

3. Main Results

The feasibility of SC photometry for the study of MPs in star clusters is tested by a comparison of the two sets of models with $Y = 0.25$ and 0.40. First, we generated the two isochrones based on the stellar models, then we chose three absolute magnitudes (or critical points) $g = 3.0$ mag, $g = 5.0$ mag and $g = 6.0$ mag from the isochrones, which are roughly located near the bottom of the RGB, the MS turnoff (MSTO) and the upper MS branches on the CMD respectively, as shown in Figure 5 for the case of NGC 2808. Stars in these phases have not experienced significant mass loss by stellar winds, therefore such stars can work as good indicators of the initial abundances that lead to MP features on the CMD in photometric observations. Moreover, stars at these locations on the CMD are not too faint to give good photometry for NGC 2808 (with corresponding visual g-band magnitudes of 18.0, 20.0 and 21.0), thus the photometric uncertainty is not an issue for the detection of predicted MP features.

We calculated the color difference at the three critical points between the two isochrones of different Y values at two passbands chosen from the CSST filters: $\Delta(X - i)$, where i is the magnitude of CSST i filter and X is the magnitude of the other. To ensure a long baseline in wavelengths to emphasize the color involving UV-bands, we used i as the subtrahend. Δ means the difference between the color indices $X - i$ calculated for the two isochrones. The results are shown in Figure 5 and Table 3. We can see that the combinations of filters with shorter wavelengths show larger deviations between the two sets of models. At all the selected g-band luminosity points on the isochrones, the color difference is significant, which decreases when the minuend filter goes from NUV toward the i filter.

In observations, the simulated color difference has to be significantly larger than the overall error budget, which has to be modeled using the instrument parameters. In general, we need to set a minimum SNR for images at all pass-bands to ensure a positive detection. A handy toolbox for the CSST mission has been made available, including the exposure time calculator (ETC) of the corresponding instrument.[9] To check if we can practically resolve those color differences caused by helium variations in NGC 2808, we need to take into account the cluster's distance modulus ($(m - M)_0 \sim 15.0$ mag). The three luminosities in Figure 5 correspond to 18, 20 and 21

[9] https://nadc.china-vo.org/csst-bp/etc-ms/etc.jsp

Table 3
Color Difference at the Three Chosen Stages Between Normal Stars and He Enriched Stars by SC/CSST Filters

Color Differences/mag	RGB	MSTO	MS
$\Delta(NUV-i)$	0.159 (0.002)	0.076 (0.006)	0.086 (0.010)
$\Delta(u-i)$	0.137 (0.003)	0.063 (0.007)	0.077 (0.011)
$\Delta(g-i)$	0.090 (0.002)	0.052 (0.006)	0.055 (0.009)
$\Delta(r-i)$	0.026 (0.002)	0.017	0.017
$\Delta(z-i)$	−0.019 (0.003)	−0.012	−0.012
$\Delta(y-i)$	−0.025 (0.004)	−0.015	−0.015

Note. Errors of the colors calculated by SNRs are listed in the parentheses beside the corresponding color difference. Strikethroughs are added to errors which are too large to detect the color difference, while others will be taken as suitable filters for detecting He-enrichment at chosen magnitudes.

visual magnitudes in g-band in observations. For the input of ETC calculations, we adopt for *NUV* and y-bands four exposures and two for other bands, with exposure time of 150 s each, just like the key parameters shown in Table 1, which are also described in Zhan (2021). By using the ETC, we calculate the SNR of each selected filter following the standard observation mode of SC, then we can further calculate the corresponding errors of color indices. For a given filter X with calculated SNR_X, the error of its color index $X-i$ is then $E_{X-i}=\sqrt{\frac{1}{\mathrm{SNR}_X^2}+\frac{1}{\mathrm{SNR}_i^2}}$ (which is also plotted as error bars in Figure 5). Afterwards, if the color difference $\Delta(X-i)$ is significantly larger than E_{X-i}, we take X as a suitable filter for detecting helium enrichment at the chosen magnitude. In this work, we adopt five times the error as the significance threshold. As is apparent in Table 3, each error is listed in the parentheses beside the corresponding color difference, with a strikethrough if the color difference is below the threshold. It is also clear that the brighter the star we observe, the easier it is to detect the He-variation. As affirmed in Figure 6, the color differences over the corresponding errors of all the filters decrease as the g-mag we choose gets fainter.

4. Discussions and Conclusions

As intensively studied by previous work, an enrichment of helium abundance will raise the mean molecular weight and decrease the opacity, and thus increase the nuclear fusion rate (Li 2021; Li et al. 2023). Stars with higher He abundance will evolve faster and be brighter and hotter in most branches (e.g., as shown in Figure 4, the helium-enriched population has a significantly hotter MS). Moreover, helium-enriched stars will populate a brighter RGB bump, as helium abundance will affect the depth of the convective envelope and change the position of chemical discontinuity (Cassisi et al. 2016). In addition, as He-enriched stars evolve faster than normal stars, they will have significantly shorter lifetimes, leading them to leave the MS and reach later phases more quickly than normal

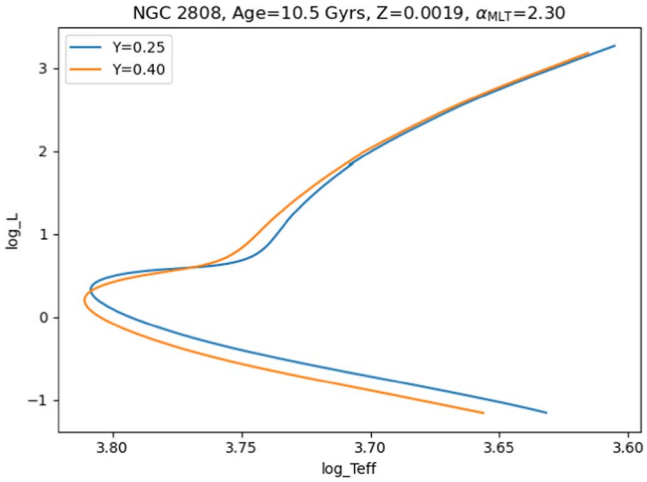

Figure 4. Model isochrones of NGC 2808 with $Y=0.25$ (blue) and $Y=0.40$ (orange) in `log_L` and `log_Teff`.

stars, therefore the helium-enriched population is always more massive at each evolutionary stage (or observed branches on the CMD). As demonstrated in Figure 7, stars with the same initial mass but different helium contents will appear in different positions on the CMD of a certain age, especially for later evolutionary stages. In other words, at a given phase in an old star cluster, helium-enriched stars will be significantly more massive than normal stars.

A typical advantage of the CSST in studying helium spread among a GC's dwarfs is its ability to reach deeper than ground-based instruments. As affirmed in Figure 5, to derive a larger color difference, it would be better to resolve the MS down to a g-band absolute magnitude of ∼21 mag, which corresponds to an apparent magnitude of $g=21.0$ mag. This is close to the background limitation (∼21.6 mag arcsec^{-2}) for ground-based telescopes, but it is brighter than the CSST's detection limit by more than 4 mag. Furthermore, because stellar surface temperature is the most sensitive parameter for helium abundance, the CSST's unique function of *UV*-band imaging allows it to study star clusters in the CMD with a maximized color baseline, which is important for resolving helium differences between stellar populations.

Comparing our results with those of Li et al. (2022), we find out that the color differences as simulated from MCI observations are in fact more significant and can provide more details than from SC. The reason is that the MCI has narrower but more filters, which enables MCI to better select spectral features of a chemical anomaly than those from SC. Meanwhile, the MCI has a few additional filters with even shorter wavelengths than the *NUV* filter of SC (e.g., F275W), which offer even longer baselines. For instance, the color difference $\Delta(M_{\mathrm{F275W}}-M_{\mathrm{F814W}})$ is ∼0.4 mag at $M_{\mathrm{F555W}}=2.0$ magnitude near the bottom of the RGB for NGC 2808. Nevertheless, SC

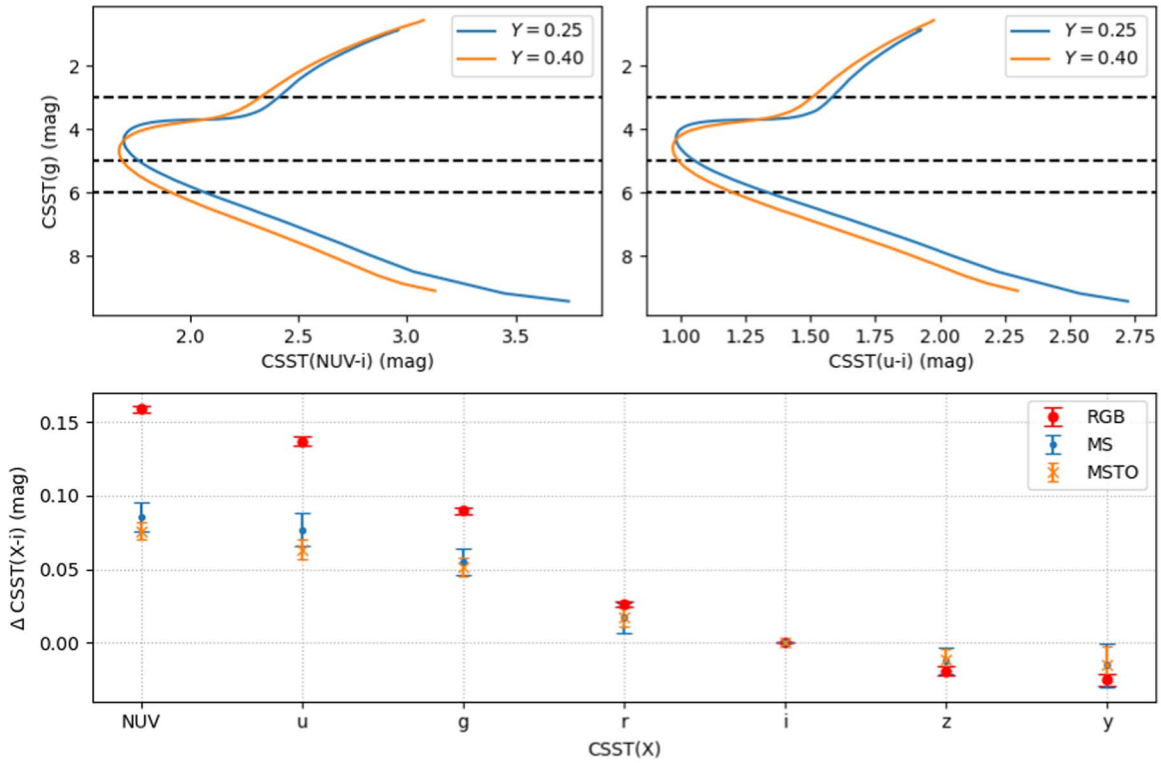

Figure 5. Top left: isochrones with $Y = 0.25$ (blue) and $Y = 0.40$ (orange) in g mag vs. $NUV-i$ color; top right: isochrones with two Y in g mag vs. $u-i$ color; bottom: color difference $\Delta(X - i)$ of two isochrones in X (filter)-i at the chosen MS, MSTO and RGB mags. Error bars show the errors of color differences calculated by ETC. See text for details.

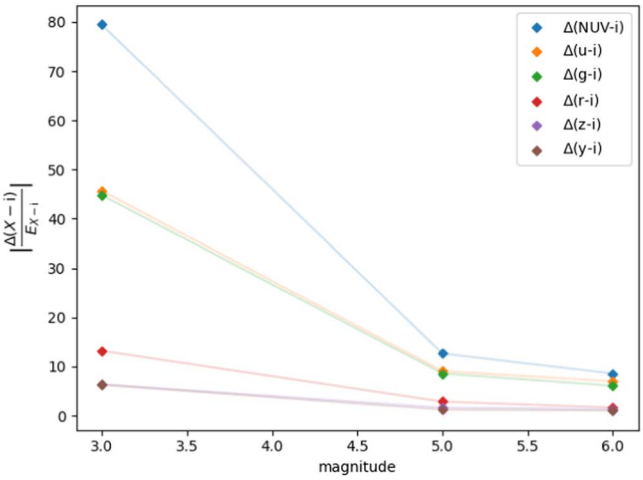

Figure 6. $|\frac{\Delta(X-i)}{E_{X-i}}|$ calculated via each filter vs. the g-mag we choose to detect the color difference.

also has advantages over MCI. The FOV of SC is about 8 times larger than that of MCI, which therefore possesses an absolute power over the latter, not mentioning that both have nearly the same spatial resolutions. For the case of NGC 2808, MCI cannot fully cover the tidal radius of the cluster even though it is already much larger than that of the HST cameras. When running an observing task with a focus on completeness of member stars, multiple observations to make a mosaic are still acceptable, but with a high price of observing time. While for the case of SC, one single image can cover a range much larger than the dynamical radius (see Figure 2). For many astrophysical research goals on targets of a size similar to that of NGC 2808, especially when the surrounding environment is important to the science of the researches, SC is an ideal instrument with a trade-off in terms of spectral coverage.

The main survey instrument, the SC on board CSST, has a great potential covering most of the cutting edge frontier topics in astrophysics. For the specific scientific goal of stellar populations and star-forming history of star clusters, its promising characteristics can be summarized into the following three aspects:

1. Compared to ground-based instruments, the forthcoming CSST can provide much deeper images (down to ∼25 mag in *NUV* and *u* passbands), which are important for studying stellar helium distributions in star clusters as these patterns commonly occur at the lower part of their MSs.

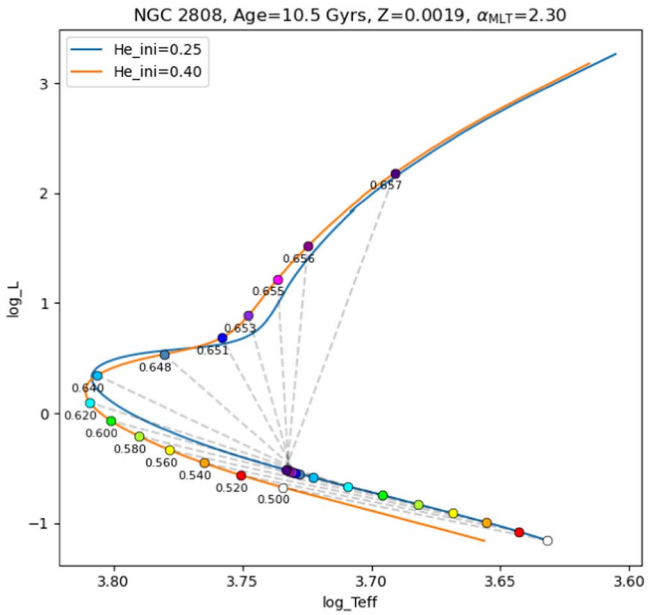

Figure 7. Examples of stars with the same initial masses on two different isochrones (both are the age of NGC 2808) with different helium contents. Stellar mass varies from 0.500 to 0.657 $M_{\odot}$. Markers with the same initial masses are colored the same and connected with dashed lines. The mass values are marked for a few points along the isochrone.

2. The unique CSST passbands of *NUV* and *u* are important for maximizing the color difference between helium normal and enriched populations.
3. The large FOV of the SC/CSST would allow studies of MPs covering different cluster structures, from the cluster core region out to the tidal tails.

Acknowledgments

This work is supported in part by China Manned Space Project with NO. CMS-CSST-2021-A08. The authors acknowledge the National Natural Science Foundation of China (NSFC, Grants Nos. 12233009, 12233013, 12073090 and 12003001).

ORCID iDs

Xin Ji https://orcid.org/0000-0002-5485-3223
Licai Deng https://orcid.org/0000-0001-9073-9914

References

Bastian, N., & Lardo, C. 2018, ARA&A, 56, 83
Bressan, A., Marigo, P., Girardi, L., et al. 2012, MNRAS, 427, 127
Cao, Y., Gong, Y., Meng, X.-M., et al. 2018, MNRAS, 480, 2178
Carretta, E., Bragaglia, A., Gratton, R. G., et al. 2009, A&A, 168, 81
Cassisi, S., Salaris, M., & Pietrinferni, A. 2016, A&A, 585, A124
Chantereau, W., Salaris, M., Bastian, N., & Martocchia, S. 2019, MNRAS, 484, 5236
Chen, Y., & Girardi, L. F. X. 2019, ARA&A, 632, A105
Choi, J., Dotter, A., Conroy, C., et al. 2016, ApJ, 823, 102
Dalessandro, E., Salaris, M., Ferraro, F. R., Cassisi, S., et al. 2011, MNRAS, 410, 694
Dolphin, A. E. 2016, DOLPHOT: Stellar photometry, Astrophysics Source Code Library, ascl:1608.013
Gong, Y., Liu, Y., & Cao, Y. 2019, ApJ, 883, 203
Gratton, R. G., Lucatello, S., Sollima, A., et al. 2013, A&A, 549, A41
Gratton, R. G., Sneden, C., & Carretta, E. 2004, ARA&A, 42, 385
Kurucz, R. L. 2005, MSAIS, 8, 14
Lada, C. J., & Lada, E. A. 2003, ARA&A, 41, 57
Li, C. 2021, ApJ, 921, 171
Li, C., & de Grijs, R. 2019, ApJ, 876, 94
Li, C., Ji, X., Wang, L., et al. 2023, arXiv:2302.10466
Li, C., Zheng, Z., Li, X., et al. 2022, RAA, 22, 095004
Marino, A. F., Milone, A. P., & Przybilla, N. 2014, MNRAS, 437, 160
Martocchia, S., Cabrera-Ziri, I., Lardo, C., et al. 2018, MNRAS, 473, 2688
Massari, D., Fiorentino, G., McConnachie, A., et al. 2016, A&A, 586, A51
Milone, A. P., Marino, A. F., Da Costa, G. S., et al. 2020, MNRAS, 491, 515
Milone, A. P., Marino, A. F., Piotto, G., et al. 2015, ApJ, 808, 51
Milone, A. P., Piotto, G., Renzini, A., et al. 2017, MNRAS, 464, 3636
Monelli, M., Hidalgo, S. L., Stetson, P. B., et al. 2010, ApJ, 720, 1225
Moreno, E., Pichardo, B., Velázquez, H., et al. 2014, ApJ, 793, 110
Niederhofer, F., Bastian, N., Kozhurina-Platais, V., et al. 2017, MNRAS, 464, 94
Piotto, G., Milone, A. P., bedi, L. R., et al. 2015, AJ, 149, 91
Piotto, G., et al. 2007, ApJ, 661, L53
Saracino, S., Bastian, N., Kozhurina-Platais, V., et al. 2019, MNRAS, 489, L97
Shetrone, M. D. 1996, AJ, 112, 1517
Tailo, M., Milone, A. P., Lagioia, E. P., et al. 2020, MNRAS, 498, 5745
Villanova, S., Piotto, G., & Gratton, R. G. 2009, A&A, 499, 755
Zhan, H. 2011, SSPMA, 41, 1441
Zhan, H. 2021, ChSBu, 66, 1290